2011

Dynamic Light Scattering and Zeta Potential of Colloidal Mixtures of Amelogenin and Hydroxyapatite in Calcium and Phosphate Rich Ionic Milieus

Vuk Uskoković
Chapman University, uskokovi@chapman.edu

Roselyn Odsinada
University of California - San Francisco

Sonia Djordjevic
University of California - San Francisco

Stefan Habelitz
University of California - San Francisco

Recommended Citation

Uskoković V, Odsinada R, Djordjevic S, Habelitz S. Dynamic light scattering and zeta potential of colloidal mixtures of amelogenin and hydroxyapatite in calcium and phosphate rich ionic milieus. *Arch Oral Biol.* 2011;56(6):521-532. doi:10.1016/j.archoralbio.2010.11.011.

Dynamic Light Scattering and Zeta Potential of Colloidal Mixtures of Amelogenin and Hydroxyapatite in Calcium and Phosphate Rich Ionic Milieus

Published in final edited form as:
Arch Oral Biol. 2011 June ; 56(6): 521–532. doi:10.1016/j.archoralbio.2010.11.011.

Dynamic Light Scattering and Zeta Potential of Colloidal Mixtures of Amelogenin and Hydroxyapatite in Calcium and Phosphate Rich Ionic Milieus

Vuk Uskoković, **Roselyn Odsinada**, **Sonia Djordjevic**, and **Stefan Habelitz**
Division of Biomaterials and Bioengineering, Department of Preventive and Restorative Dental Science, University of California, San Francisco

Abstract

The concept of zeta-potential has been used for more than a century as a basic parameter in controlling the stability of colloidal suspensions, irrespective of the nature of their particulate ingredients – organic or inorganic. There are prospects that self-assembly of peptide species and the protein-mineral interactions related to biomineralization may be controlled using this fundamental physicochemical parameter. In this study, we have analyzed the particle size and zeta-potential of the full-length recombinant human amelogenin (rH174), the main protein of the developing enamel matrix, in the presence of calcium and phosphate ions and hydroxyapatite (HAP) particles. As calcium and phosphate salts are introduced to rH174 sols in increments, zeta-potential of the rH174 nanospheres is more affected by negatively charged ions, suggesting their tendency to locate within the double charge layer. Phosphate ions have a more pronounced effect on both the zeta-potential and aggregation propensity of rH174 nanospheres compared to calcium ions. The isoelectric point of amelogenin was independent on the ionic strength of the solution and the concentration of calcium and/or phosphate ions. Whereas rH174 shows a higher affinity for phosphate than for calcium, HAP attracts both of these ions to the shear plane of the double layer. The parallel size and zeta-potential analysis of HAP and rH174 colloidal mixtures indicated that at pH 7.4, despite both HAP and rH174 particles being negatively charged, rH174 adsorbs well onto HAP particles. The process is slower at pH 7.4 than at pH 4.5 when the HAP surface is negatively charged and the rH174 nanosphere carries an overall positive charge. The results presented hereby demonstrate that electrostatic interactions can affect the kinetics of the adsorption of rH174 onto HAP.

Introduction

Surface charge of particles in sols has been used for centuries to regulate the stability of colloidal suspensions[1,2,3]. The ancient Egyptians used to render many colloids, from clay to ink, stable by electrostatic means, without being aware of that[4,5]. Built on the basis of Gouy-Chapman model of the particle-solution interface, DLVO theory developed in 1940s by Derjaguin and Landau, and Verwey and Overbeek, separately, explained the stability of colloids by drawing a balance between the repulsive electric double layer forces and the attractive, short-range van der Waals forces. Ever since the propositions of this theory, it has been used as the theoretical basis for controlling the stability of colloidal dispersions in various technologies. An essential and easily measurable quantity used to control the

intensity of the repulsive electrostatic interaction between the naturally charged colloidal particles is zeta-potential (ζ-potential).

As far as the biochemical systems are concerned, it is known that enzyme-ligand binding is favored under conditions of electrostatic attraction[6]. Also, enzyme immobilization is known to depend not only on the chemical interaction specificity, but also on the difference in the surface potentials between the enzyme molecule and the matrix carrier[7]. Electrostatic effects have been regularly used for the electrophoretic separation of peptides, and the protein adsorption has been shown to be directly dependent on the magnitude of the difference between the ζ-potentials of the protein and the adsorbent[8]. Deviations of ζ-potential of cells from the normal range of values have been used as an indicator of membrane abnormalities[9]. Charge on the cell membrane, originating from phosphoryl and carboxyl groups of macromolecules that constitute it[10], can be manipulated to prevent cellular aggregation, which is an effect detrimental for cellular electrophoresis techniques[11]. It was recently proposed that ζ-potential may play a role in viralhost interactions[12], whereas ζ-potential of polioviruses was used as a control parameter during their removal from contaminated waters[13]. Zeta-potential has also been used to explain the effect of ions on coagulation in blood, including the effect of thrombosis[14]. Recently, the same concept was applied to explain the aggregation of cholesterol particles, demonstrating how a control over ζ-potential may be used to prevent the formation of pathological cholesteric deposits, including atherosclerotic plaque and gallstones[15,16]. The idea to manipulate surface charges of interacting species in order to generate complex soft matter morphologies has been, however, pursued to a lesser extent.

The reason behind studying the interaction between amelogenin (AMG), the main protein of the developing enamel matrix, and hydroxyapatite (HAP), the main mineral component of hard tissues, lies in its relevance for the process of morphogenesis of tooth enamel, known as amelogenesis. During this process, AMG self-assembles into an intricate protein network composed of nanospheres and/or nanofibers that guide the growth of bundles of elongated HAP crystals. There are indications that the first step in the self-assembly of AMG is conditioned by a narrow window of pH values at which nanospheres of different AMGs (e.g., the full-length and the proteolytically cleaved ones) are oppositely charged[17]. A former study demonstrated that the formation of nanofibrous AMG entities was fostered under conditions at which the full-length AMG nanospheres and those composed of the largest proteolytic product of the enzymatic degradation of AMG by means of matrix metalloproteinase 20 (MMP-20), one of the two main proteases of the enamel matrix, carry opposite charges[17]. As for the protein-mineral interaction, the exact nature and conditions for protein adsorption/desorption to and from the mineral surface are not precisely defined. By understanding the mechanism of this process, an insight into the fundamental nature of protein-mineral interactions that govern biomineralization processes in general could potentially be gained, altogether with a prospect of enabling more superior clinical treatments for restoring the diseased enamel.

In our previous work, we studied the effect of pH on the particle size and ζ-potential of full-length recombinant human AMG (rH174) and the two largest recombinant products of the digestion of AMG by means of MMP-20[18]. The tendency of the protein nanoparticles to aggregate into micro-sized and easily segregating entities was observed in the mildly acidic pH range, 4 – 7, above and below which the protein retained the form of 20-40 nm sized spheres. The tendency of the protein particles or molecules to aggregate in the weakly acidic pH range has previously been observed for a 340 kDa blood plasma protein, fibrinogen[19]. In this study, we have focused on following a change in ζ-potential upon the addition of different ionic (Ca^{2+}, $H_xPO_4^{x-3}$) and particulate (HAP) species. The content of this work is therefore divided into two parts. In the first part, we report the effect of the addition of

calcium and phosphate ions to rH174 sols. The second part is the study of the interaction between HAP and rH174 by means of simultaneous particle size and ζ-potential analyses. Since specific properties with respect to particle and/or molecular size and aggregation propensities are shared by different proteins, the purpose of this study is applicable to understanding multiple other protein-protein and protein-mineral interactions, primarily those relevant to biological mineralization.

Materials and Methods

The protein and mineral suspensions were analyzed by means of a Zetasizer Nano Series (*Malvern, UK*) with the measurement range of 0.6 nm – 3 μm. Unless otherwise noted, 0.2 mg rH174 was dissolved in a low pH aqueous solution containing 30 mM Tris or Bis-Tris buffer and 100mM KCl. This sample was then vortexed and centrifuged, and the supernatant dispersion was used for the dynamic light scattering (DLS) analysis. The desired pH was reached by adding small volumes (1 – 10 μl) of 2 M HCl/KOH. Measurements were taken at calcium ($CaCl_2$) or phosphate (KH_2PO_4) concentrations of 0.1, 0.3, 0.5, 1, 1.5, 2, 3 and 8 mM. The pH range of 2-10 was covered at intervals of one pH unit, thus analyzing rH174 in both the monomeric and particulate form. Samples were analyzed for particle size and ζ-potential in the same runs and immediately upon mixing the components, resulting in t = 3 min as the earliest time point in the time-dependent analyses. The volume of each suspension was 1 ml and the results of each measurement were averaged over 100 runs at acquisition times of ~ 10 s, with the data analysis software yielding the statistically averaged size distribution by particle number as the output. The measurement temperature was 25 °C, unless noted otherwise. Universal dip cell (Malvern, UK) with a removable palladium electrode and the spacing of 2 mm in disposable glass cuvettes was used for the measurements. The voltage was manually set to 20 V and the short-pulse monomodal measurement setting was applied. To eliminate the effect of large particulate impurities, number size distribution was used for derivation of the particle size reported hereby. The particle sizes reported present hydrodynamic diameters. The average standard deviation (SD) for size and ζ-potential of AMG and HAP particles, depending on polydispersity, impurity content and inherent instability of the sols, was determined on the sample size, N = 100, as equal to: $SD(d_{AMG}) = \pm 8$ % in the 1 – 100 nm range and ± 25 % in 0.1 μm – 3 μm range; $SD(d_{HAP}) = \pm 15$ % in the entire particle size range; $SD(\zeta_{AMG}) = \pm 5$ % and $SD(\zeta_{HAP}) = \pm 12$ %. The isoelectric points (IEPs) were determined by interpolation of mean ζ -potential values at the zero value.

Recombinant human rH174 was previously synthesized by expression in BL21(DE3) plysS *Escherichia Coli*[2021]. Egg yolk phosvitin was purchased from *Sigma*, and HAP powder was prepared by precipitation from aqueous solution according to the procedure described previously[22]. HAP used in this study was predominantly B-type carbonated apatite, although carbonate-for-hydroxyl substitution was present too, whereas sodium and magnesium were two other main impurities. Together with Ca/P molar ratio of 1.6, this particular HAP showed high similarity to the biological apatite[23]. X-ray diffraction analyses of HAP confirmed pure apatite, while the lattice parameters were undetermined. For the experiments in which rH174 was added in increments to the initial HAP suspensions, the following procedure was applied. One ml of the solution comprising 20 mM Tris/HCl and 150 mM KCl at pH 7.55 was added to 1 mg of HAP, vortexed and centrifuged at 4000 rpm for 3 min. The supernatant dispersion was then extracted, set to pH 7.40 +- 0.02 or 4.50 +- 0.02, and analyzed. The same buffered electrolyte solution was added to 0.4 mg of rH174, followed by vortexing and centrifugation. The supernatant was separated, diluted twice and set to pH 8.00 +- 0.02, so as to ensure the nanosized and stable nature of the dispersed protein particles. The protein dispersion was then added in increments to the HAP sol and analyzed in the dip cell for the particle size and zeta potential. The desired pH was maintained during

the measurement. In order to eliminate the error due to extensive pH fluctuations and instability, Tris/Bis-Tris/HCl was used as the buffer in the 5.8 – 9.3 pH range and added to samples equilibrated at other pH values for reproducibility purposes. The extent to which the organic buffer exhibited specific adsorption is unknown, although comparisons of Tris-free and Tris-containing samples in the phosphate buffered zone showed no significant change of particle size and ζ-potential values. The analysis of aqueous 20 mM Tris/Bis-Tris solution resulted in a 60 nm peak, although with 30 kcounts (photons detected per second) at 100 % laser intensity. In comparison, a typical rH174 sample yielded circa 300 kcounts at 3 % of laser intensity, signifying a negligible effect of Tris/Bis-Tris on the DLS signal during the analysis of HAP and rH174 sols. Quantitative analyses of the ionic content with respect to calcium and phosphate were done using a calcium ion-selective electrode (*pHoenix*) and atomic absorption spectrophotometry (*Milton Roy, Genesys 5*), respectively. Samples for the electron microscopy analysis were prepared by depositing a droplet of vortexed HAP/AMG sols onto a glow-discharged carbon grid (Electron Microscopy Sciences, Hatfield, PA) and staining the protein with phosphotungstic acid. Electron microscopy analysis was done on both pure HAP sols and those containing mixtures of HAP and AMG using a 200kV FEI monochromated F20 UT Tecnai transmission electron microscope (TEM).

Results and discussion

a) Effects of Calcium and Phosphate on Particle Size and Zeta Potential of rH174

Owing to a comparatively large proportion of hydrophobic side chains within its primary structure and a partly amphiphilic nature, as implied by the highly hydrophilic sequence of 13 amino acids at the C-terminal (Fig.1a), rH174 tends to form nanospheres in aqueous solutions even at concentrations lower than 0.01 mg/ml (Fig.1b). C-terminal is known to be present on the nanoparticle surface[24], indicating a possible micelle-like structure of these self-assembled colloidal entities[25]. Also, the full-length AMG molecules formed tightly connected, elongated, high-aspect ratio assemblies comprised of smaller spheres under certain conditions[26]. These protofibrous AMG entities (Fig.1c) are thought to present the first step in the formation of more complex architectures that guide the growth of elongated enamel crystals.

Fig.2 demonstrates the typical shapes of ζ-potential vs. $[Ca^{2+}/H_xPO_4^{x-3}]$ curves, whereby Figs.3a and 3c display its dependence on the pH. As can be seen from Fig.2, the additions of $H_xPO_4^{x-3}$ and Ca^{2+} have different effects on ζ-potential of rH174. Whereas in case of the $H_xPO_4^{x-3}$ addition, a continuous drop in ζ-potential is observed for all the pHs analyzed, in case of the Ca^{2+} addition an initial drop is observed in the concentration range of 0 – 0.1, 0 – 0.2, 0 – 2, 0 –0.4, and 0 – 8 mM for samples at pHs 10, 9, 8, 7 and 2, respectively, after which a region typified by a steady rise in ζ-potential follows. This trend of the initial decrease in ζ-potential at low ionic concentrations suggests that negatively charged ions tend to locate themselves on the particle side of the slipping plane despite the fact that rH174 is negatively charged at pH > 7. It is only the sample analyzed at pH 2 that yields a thorough decrease in ζ-potential following the addition of Ca^{2+} (Fig.3a). As indicated by the increase in the particle size (Fig.3d), KH_2PO_4 has a tendency to induce aggregation more easily than $CaCl_2$. This is most strikingly observed at pH 2 when after $[KH_2PO_4] = 0.25$ mM is reached the aggregation of the nanospheres takes place, initiating the segregation of the protein from the solution. In contrast, at the same pH adding Ca^{2+} up to 8 mM does not produce any significant change in the particle size. The latter remains below 100 nm at all pHs except within the $4 \leq pH \leq 7$ aggregation zone, which was previously established for rH174[18]. Also, as shown in Fig.3b, the particle size at pH 2 for $[Ca^{2+}] = 0 – 8$ mM approaches the size of rH174 monomers. Namely, with the molecular weight of 19.8 kDa and density of 0.78 g/ml, Perrin factor for rH174 equals 1 for the hydrodynamic diameter of 4 nm. Reliable zeta-potential measurements were hindered in the given pH zone (4 – 7) due to instability of the

rH174 sols. The salting out of rH174 was most obvious at the very boundary of the aggregation zone, at pH 7, where although the pure rH174 suspension exhibited particle size of less than 100 nm, even minor additions of $CaCl_2$ or KH_2PO_4 (< 1 mM) induce rapid destabilization of the sols and increase of the particle size up to the micrometer range.

The higher propensity of KH_2PO_4 to aggregate rH174 compared to that of $CaCl_2$ is in disagreement with the general nature of the Hofmeister series[282930]. According to it, the following ions are arranged in the direction of their increasing destabilization (aggregation or unfolding) of proteins:

$$F^- = SO_4^{2-} < \mathbf{HPO_4^{2-}} < CH_3COO^- < \mathbf{Cl^-} < NO_3^- < Br^- < ClO^{3-} < I^- < ClO^{4-} < SCN^- NH^{4+} < K^+ < Na^+ < Li^+ < Mg^{2+} < \mathbf{Ca^{2+}} < CH_6N_3^+$$

Therefore, one can conclude that there is a specific tendency of phosphate ions to adsorb to rH174 and promote its aggregation. On the other hand, rH174 is able to rearrange the calcium ions across the particle volume and surface in such a way that the particles resist aggregation. The reason for this effect may be that the protein *per se*, as analyzed in this study, possesses a very specific aggregated form, which is at the same time highly dispersable (i.e., nanospheres). However, numerous other proteins, including those that control Ca^{2+} levels in blood plasma, which is supersaturated with respect to HAP, exhibit resistance to aggregation for the range of $[Ca^{2+}]$ used in this work. Saliva proteins are similarly able to sequester Ca^{2+}, and we can hypothesize that such an ability to controllably seize Ca^{2+} from the solution is directly connected to the role of AMG in enamel mineralization. Ca^{2+} may bind more tightly and selectively to rH174, whereas $H_xPO_4^{x-3}$ diffuses in the shear plane, as indicated by results shown in Fig.4. Namely, a drop in $[Ca^{2+}]$ from the initial 1.6 mM to 1.1 mM was detected following mixing 1.6 mM $CaCl_2$ and 1.0 mM KH_2PO_4 with 0.4 mg/ml rH174 over the first 8 hours. The level of phosphates similarly drops, from the initial 1.0 mM to 0.7 mM, upon mixing rH174 with both Ca^{2+} and HPO_4^{2-}/$H_2PO_4^-$ ions; otherwise, as shown in Fig.4, free $H_xPO_4^{x-3}$ concentration in solution stays unchanged at 1.0 mM after adding 0.4 mg/ml rH174 to it and aging for up to 6 h, indicating no binding of phosphates to the protein. An immediate drop from $[Ca^{2+}]$ = 1.60 mM to $[Ca^{2+}]$ = 1.47 mM is observed following mixing of the given amount of $CaCl_2$ with 0.4 mg/ml rH174 (Fig.4). The fact that $H_xPO_4^{x-3}$ ions have a higher affinity towards entering the double layer of ions around rH174 nanospheres also corroborates the set of biomimicry experiments of rH174-controlled epitaxial growth of enamel-resembling apatite wherein higher crystal growth levels and rates (at lower values of supersaturation ratio too) were observed when high initial $[H_xPO_4^{x-3}]$ was used compared to high $[Ca^{2+}]$. The ability of AMG to guide the crystal growth of apatite during amelogenesis may thus be conditioned by the strong and selective binding of Ca^{2+} to the AMG nanoparticles, whereas $H_xPO_4^{x-3}$ tends to be positioned within the shear plane and possesses a more diffusive character. Calcium ions thus supposedly act as nucleation sites, as implied by the preferential and precisely located anchoring of Ca^{2+} onto AMG. Also, 6 Ca ions bind to each rH174, according to Le *et al.*[31], which implies that 0.06 mM Ca^{2+} would be required to saturate 0.2 mg/ml rH174, assuming that all of its active sites are solvent-exposed, which is not necessarily true owing to the protein folding and hydrophobicity-driven aggregation. In view of that, only a minor change in ζ-potential may entail a total saturation of rH174 molecules with Ca^{2+}.

Looking at sheer ζ-potential values, one can conclude that $H_xPO_4^{x-3}$ has a more pronounced effect on the ζ-potential change. Aggregation induced by $H_xPO_4^{x-3}$ also corresponds to higher ζ-potentials compared to non-aggregated samples. Despite the fact that calcium ions have contributed to bringing ζ-potential closer to IEP whereas phosphate ions were shifting it in the opposite direction, of a supposedly greater stability, $H_xPO_4^{x-3}$ induced a higher

aggregation propensity of the rH174 nanospheres compared to Ca^{2+}. The reason behind the more evident effect of $H_xPO_4^{x-3}$ on both zeta-potential and the aggregation propensity of the nanospheres may lie in its higher ionic charge. With continued addition of $H_xPO_4^{x-3}$ to rH174, the ζ-potential tends to reach a plateau, presumably corresponding to the compressed diffuse layer and the saturated Stern layer of the particles. A similar but less pronounced trend is observed in case of Ca^{2+} too, and a plateau is reached at ionic concentration of ~ 5-6 mM.

Fig.5 demonstrates that the aggregation of 20-40 nm sized rH174 spheres occurs at pH < 8 for $[H_xPO_4^{x-3}] > 0.1$ mM. For $[H_xPO_4^{x-3}] \leq 0.1$ mM, the particles de-aggregate at pH = 3. The cause for aggregation of the particles at pH 2 for $[H_xPO_4^{x-3}] \geq 1.5$ mM lies in higher ionic strength of the background electrolyte compared to pH 3; ζ-potential, on the other hand, stays at a plateau in the pH range between 1 and 3[18]. As previously reported, pure rH174 in 130 mM KCl and 20 mM Tris/HCl exhibits the aggregation "window" at pH ~ 4 – 7[18]. The presence of Ca^{2+} and $H_xPO_4^{x-3}$ leads to widening of this zone due to the "salting out" effect they induce. Once located within the double layer region, $H_xPO_4^{x-3}$ induces aggregation of the nanospheres more effectively than divalent Ca^{2+}, as in accordance with the aforementioned Hofmeister series. This aggregation made it especially difficult to measure the hydrodynamic diameters at pH range 4 -7. As for Ca^{2+}, the effect of widening the aggregation zone at mildly acidic pHs is less pronounced. At pH > 8, rH174 particles are nanosized (< 100 nm), although a lack of stability is observed for pH 8 at high $[HPO_4^{2-}]$. This also means that negatively charged nanospheres turn out to be more resistant to the "salting out" effect than positively charged ones. This is consistent with the fact that biological entities are typically dispersed on the negative side. In case of cells, for example, this is so because of the negatively charged membrane glycoproteins. Another fundamental reason is the lower mobility of OH^- ions than protons, which renders the former to possess a higher tendency to be adsorbed on the particle surface.

The IEP of rH174 did not change significantly with the addition of Ca^{2+} or $H_xPO_4^{x-3}$ in the range of 0 – 8 mM for each of the ions. These results agree with the many times evidenced independence of the IEP on the ionic strength of the medium (unlike ζ-potential), provided the background electrolyte is inert. Hydrodynamic diameters of rH174 particles were shown to be independent on the protein concentration in the range of 0.01 – 3.5 mg/ml at pH 4 - 7.

Fig.6 displays the effect of adding $CaCl_2$ and KH_2PO_4 to rH174 dispersions that already contained different amounts of $H_xPO_4^{x-3}$ (0.5 and 2 mM) and Ca^{2+} (1 and 3 mM), respectively. Whereas the typical shape of the ζ-potential vs. $[Ca^{2+}]$ curve remains unchanged compared to that seen in the absence of $H_xPO_4^{x-3}$ species (Fig.2), the ζ-potential vs. $[H_xPO_4^{x-3}]$ curve reverts its trend of decreasing ζ-potential already after 0.2 – 1 mM of added KH_2PO_4. As the shape of ζ-potential vs. $[Ca^{2+}/H_xPO_4^{x-3}]$ curves shown in Fig.6 resembles more that which represents titration with $CaCl_2$ rather than with $HPO_4^{2-}/H_2PO_4^-$, this may indicate that Ca^{2+} is more critical interfacial ion for rH174 than $HPO_4^{2-}/H_2PO_4^-$. In accordance with the aforementioned observation that the rH174-controlled crystal growth of apatite is more enhanced at low $[Ca^{2+}]$ and high$[H_xPO_4^{x-3}]$ than *vice versa*, a formation of fine amorphous or crystalline entities of calcium phosphate may have taken place under conditions at which Ca^{2+} was already present in the system before the addition of KH_2PO_4 started, which is exactly the case in which the deviation from the trend observed in single-ion titration was detected (Fig.6b).

b) Particle Size and Zeta Potential Analysis of Colloidal Mixtures of rH174 and HAP

Fig.7a-b compares the ζ-potential of HAP and rH174 at pH 7.40 +- 0.02, respectively, following the addition of $CaCl_2$ and KH_2PO_4 up to 15 mM. In case of HAP, a shift towards positive side of ζ-potential values is observed following the addition of Ca^{2+} and the

opposite shift is detected following the addition of KH_2PO_4, suggesting that both calcium and phosphate species tend to preferentially localize within the surface of HAP particles. In contrast, a trend in ζ-potential change observed for rH174 at pH 7.4 is in agreement with the one reported in the previous section. It demonstrates a preferential adsorption of negatively charged ions ($H_xPO_4^{x-3}$, Cl^-) onto rH174 particles compared to those of Ca^{2+} and K^+.

A hydrated layer containing relatively mobile ionic species is assumed to be present on the surface of HAP particles in the solution. The composition of this layer would be subject to change depending on pH and ionic content of the medium. This high surface ionic mobility is thought to be responsible for the relatively high electrical conductivity exhibited by HAP[32]. Hence, an intensive exchange of ions between the solution and HAP particles is expected to take place, implying that all of the constitutive ions will be preferentially located in the vicinity of the particle surface where they can have an effect on the ζ-potential. It is known that the drastic effect of F^- in the suspension medium on the ζ-potential can be explained only by assuming its incorporation in the crystal lattice of the apatite[33]. This may explain why the composition of the surface of suspended or precipitated HAP particles is different compared with their bulk composition, even in situations when the solution is supersaturated with respect to HAP so as to prevent its slow dissolution. This ion-exchange propensity of HAP may be another factor crucial in providing the cellular environment with an access to the constituent ions for the sake of facile bone remodeling or consumption of ions for other purposes (as bone also acts as a frequently accessed mineral reservoir)[32]. On the other hand, despite the high mobility of surface ions, HAP is typified by its sparsely soluble nature and slow crystal growth even at very high S, which implies an intricate ordering of ionic layers (that is, the solid surface layer of the particle and the double-layer of ions surrounding it) that contribute to surface charges and its propensity for restructuring depending on ionic environment. Consequently, it has been shown that the methods of preparation and changes in stoichiometry (Ca/P ratio) significantly affect IEP of HAP[34]. Pure HAP powders precipitated in acidic conditions were thus shown to possess 1 – 3 pH units lower IEPs compared to those precipitated from alkaline solutions[35]. It is natural to expect that the structure of the mobile surface layer would depend on the physical and chemical conditions under which the particles were prepared, and this effect can be invoked to explain a large discrepancy between IEP and surface potential values of HAP particles in the literature. Thus, whereas some studies report negatively charged particles in the entire pH range in which HAP is the stable phase[36], others report IEP values at anywhere between 5 and 7.5, below which the particles become positively charged[3738]. There are, however, reports[39] on IEP of HAP suspensions detected at pHs as high as 10. This all speaks in favor of complex surface charge properties of HAP, which often present the first steps in specific crystal growth interactions between organic and inorganic phases.

From Fig.8a which displays results obtained when adding rH174 in increments to a stable HAP sol at pH 7.40 +- 0.02, we can see that already at 0.018 mg/ml, which was the lowest [rH174] at which the DLS analysis could be carried out with high quality, the 20 nm rH174 peak disappears in favor of a 1.4 μm peak. As the 20 nm peak is not visible in the mixture of HAP and rH174 of the same [rH174], it clearly suggests that rH174 adsorbs on the HAP surface. At all other [rH174], extending up to 0.16 mM, no 20 – 40 nm rH174 peak was observed, indicating a thorough adsorption of rH174 in the entire concentration range analyzed. The decrease in ζ-potential of HAP with increasing [rH174], shown in Fig.8b, furthermore confirms binding of the protein to the apatite surface. Whereas the ζ-potential of pure HAP was measured to be -17 mV, the one for pure rH174 was, according to our previously published results, in the range of – 5 to – 8 mV and independent on the protein concentration (from 21 nm at [rH174] = 0.018 mM to 29 nm at [rH174] = 0.32 mM). With the addition of rH174, ζ-potential of HAP moves towards the one of rH174. In couple with the size results, this observation indicates a full coverage of HAP particles after the final

[rH174] = 0.16 mM is reached. The HAP particle size larger than 1 μm observed at 0.01 mM < [rH174] < 0.07 mM suggests that rH174 acts as a flocculant in that particular concentration range. This was confirmed by using another, commercially available HAP powder (*Berkeley Advanced Biomaterials, Inc.*) with the precisely defined particle size. In that set of experiments, rH174 proved as a flocculant at [rH174] = 0.14 – 0.22 mM by increasing the measured particle size from the initial 200 nm to more than 1 μm. This flocculation effect was, however, observed only at 7 < pH < 10. Also, flocculants act as such even when not thoroughly coating the particles. As a result, the zeta-potential at low [rH174] corresponds to the average of HAP and rH174. At higher [rH174], HAP surface becomes more thoroughly covered, resulting in the ζ-potential approaching the value of pure rH174, as shown in Fig.8b. No change in the particle size was detected during extensive aging, indicating a dispersive character of rH174 at [rH174] > 0.1 mg/ml, although it completely adsorbs onto HAP. Neither did ζ-potential significantly change during 4-day aging (- 8 to - 9 mV).

From Fig.9a which displays results obtained when adding rH174 abruptly at concentration that equals the final one in the experiment involving the incremental addition thereof ([rH174] = 0.16 mM), we can see that the adsorption of rH174 nanospheres onto HAP particle surface at pH 7.4 is a time-dependent phenomenon. During the first hour of aging, the average particle size according to the particle number distribution corresponds to the one of 20 –40 nm sized rH174 particles, after which this peak disappears in favor of the one associated with the order of magnitude of the initial size of HAP particles, indicating a complete binding. Meanwhile, the ζ-potential did not show any significant change, corresponding throughout the entire aging time to that of rH174, as visible from Fig.9b. This is understandable since these particles outnumbered the HAP ones and were thus the primary entities that contributed to the electrophoretic mobility measured.

The HAP particles used in this study were shown to have negative values of ζ-potential at the entire pH range of the stability of HAP, that is, 4 – 11. In contrast, our previously reported analyses came to the conclusion that rH174 exhibits an IEP at mildly acidic values and at lower pHs becomes positively charged. Such a behavior is typical for proteins in general, which possess intrinsic charges as the result of selective dissociation of the titratable amino acid side chains and the carboxyl and amino groups at C- and N- terminals, respectively. Correspondingly, at pH 7.4, the HAP particles applied in this study and rH174 nanospheres would both possess negatively charged surfaces. Despite the negative ζ-potential of both entities, the nanosized rH174 spheres were shown to adsorb onto HAP nanoparticles, as evident from Figs.8 and 9. Transmission electron micrographs presented in Fig.10 demonstrate sharp particle edges in pure HAP samples and a protein layer surrounding HAP particles after they were mixed with rH174 at pH 7.4. The elemental analysis given in the inset of Fig.10a confirms the uniformity of the calcium content (white dots) of the analyzed particles.

To test whether the kinetics of the adsorption of rH174 onto HAP particles would be different if these two surfaces were of opposite charges, we carried out a similar experiment as the one shown in Fig.9, but at pH 4.5, at which rH174 nanospheres were positively charged and HAP would remain negatively charged. From the obtained results, shown in Fig.11a, one can see that the size peak that corresponds to rH174 (75 nm in this case, as this pH value lies close to the lower boundary of the pH 4 – 7 aggregation zone) is not visible even at the lowest aging times, indicating a more rapid adsorption of rH174 onto HAP particles under conditions at which these two interacting entities are oppositely charged. Likewise, whereas the ζ-potential of pure HAP at pH 4.5 was measured as - 5.2 mV and the one of pure rH174 at the same pH was + 5.4 mV, the resulting value for the HAP/rH174 mixture remained positive, in the range of 4 – 10 mV during the 11 h aging time, yielding

another indication in favor of the adsorption of rH174 onto HAP. This certainly proves the hypothesis that electrostatic interactions, controllable via the ζ-potential parameter, can affect the kinetics of the adsorption of rH174 onto HAP.

The fact that the initial size of HAP and rH174 particles was measured to be 115 and 75 nm, respectively, whereas the size of the particles resulting after the adsorption of rH174 onto HAP was between 180 and 400 nm may suggest that rH174 monomers may present the dominant adsorbed entities rather than the nanospheres *per se*. Such an indication may be supported by the recent findings that the AMG adsorbates on apatite surface were either monomers or oligomers, significantly smaller than the original nanospheres[40]. The hump in the ζ-potential vs. time curve shown in Fig.11a was repeatedly observed and could be the sign of a conformational change of the adsorbed protein. Aoba *et al*. have shown earlier that AMG adsorbs well onto HAP in the pH range of 6.0 – 7.4[41]. There is also evidence that a change in the protein conformation takes place upon the binding of AMG onto HAP[42], which is also supported by the finding of more cleavage sites for AMG bound to HAP surface than for AMG in the solution[43].

The results presented so far were obtained from aqueous suspensions initially undersaturated with respect to HAP. A set of additional analyses was carried out at different pHs and under conditions at which the ionic content of the surrounding medium was set to supersaturation ratio with respect to HAP equal to one. The main difference compared to the results obtained for the undersaturated solutions was lower values of ζ-potential of HAP/rH174 induced by high concentrations of Ca^{2+} and $H_xPO_4^{x-3}$. Namely, as shown in part *a*, it is primarily anions, that is $H_xPO_4^{x-3}$ and Cl^-, that tend to approach the AMG particle surface, shifting its ζ-potential to the negative side. Whether rH174 is freely suspended or adsorbed onto HAP particles, the effect of high concentrations of anions will contribute to lowering of the resulting ζ-potential values. As noted previously, combination of a highly mobile surface layer of ions and a sparsely soluble surface results in an extraordinary complexity of charges that surround HAP particles, including both the crystal surface and the double layer of ions. This was furthermore evidenced in the experiment in which a markedly lower ζ-potential was detected upon mixing phosvitin, a highly phosphorylated protein, with the HAP sol, as shown in Fig.11b. As the medium was in this case rich in $H_xPO_4^{x-3}$, the common ion effect dictated selective dissolution of primarily Ca^{2+} from the HAP surface, endowing the latter with a more negative net charge.

Conclusion

A parallel hydrodynamic diameter and ζ-potential analysis such as the one reported here is proven as useful in examining the fundamental properties of the interaction of the given colloidal phase, rH174, either with solutes (Ca^{2+} and $H_xPO_4^{x-3}$), or with other particulate phases (HAP). As calcium and phosphate salts are introduced to rH174 sols, ζ-potential of the protein particles is more affected by the negatively charged ions ($H_xPO_4^{x-3}$, Cl^-), suggesting their tendency to locate within the double layer. Only at concentrations higher than 0.2 – 2 mM, depending on the pH value, calcium ions become dominant species in the double layer, inducing an increase in the ζ-potential. Despite the fact that calcium ions have contributed to bringing ζ-potential closer to IEP and phosphate ions were shifting it in the opposite direction, of a supposedly greater stability, $H_xPO_4^{x-3}$ induced a higher aggregation propensity of the rH174 nanospheres compared to Ca^{2+}. The IEP of rH174 was shown to be independent on the ionic strength of the solution. Whereas the hydrodynamic sphere of rH174 shows a higher affinity for $H_xPO_4^{x-3}$ over Ca^{2+}, HAP attracts both Ca^{2+} and $H_xPO_4^{x-3}$ ions to the shear plane of the double layer. Changes in both the particle size and the ζ-potential indicate that at pH 7.4, despite both HAP and rH174 particles being negatively charged, rH174 adsorbs well onto HAP. However, this process is slower at pH

7.4 than at pH 4.5 when HAP and rH174 surfaces carry opposite charges. Electrostatic interactions can therefore affect the kinetics of the adsorption of rH174 onto HAP. Zeta-potential can be analyzed to estimate the intensity of this electrostatic interaction, which can be controlled by pH and ionic concentrations.

Acknowledgments

Presented were the results of a study supported by NIH/NIDCR grants R01-DE017529 and R01-DE015821. This work was partly performed at NCEM, which is supported by the Office of Science, Office of Basic Energy Sciences of the U.S. Department of Energy under Contract No. DE-AC02-05CH11231 (#1375). The authors would like to thank Fan Yang for a few DLS measurements incorporated within this study, and Li Zhu and Joseph Mendoza for the synthesis of rH174.

References

1. Kosmulski, M. Surface charging and points of zero charge. CRC Press; Boca Raton, FL: 2009.
2. Shaw, DJ. Introduction to Colloid and Surface Chemistry. (Butterworth Heinemann; Oxford, UK: 1992.
3. Uskokovic V. Theoretical and Practical Aspects of Colloid Science and Self-Assembly Phenomena Revisited. Reviews in Chemical Engineering. 2007; 23:301–372.
4. Lyklema, J. Fundamentals of Interface and Colloid Science, Volume IV: Particulate Colloids. Academic Press; London, UK: 2005.
5. Shchukin, ED. Colloid and Surface Chemistry. Elsevier; Amsterdam, NL: 2001.
6. Wade RC, Gabdoulline RR, Ludemann SK, Lounnas V. Electrostatic steering and ionic tethering in enzyme-ligand binding: Insights from simulations. Proceedings of the National Academy of Sciences. 1998; 95:5942–5949.
7. Schultz N, Metreveli G, Franzreb M, Frimmel FH, Syldatk C. Zeta potential measurement as a diagnostic tool in enzyme immobilisation. Colloids and Surfaces B: Biointerfaces. 2008; 66:39–44.
8. Cai K, Frant M, Bossert J, Hilderbrand G, Liefeith K, Jandt KD. Surface functionalized titanium thin films: Zeta-potential, protein adsorption and cell proliferation. Colloids and Surfaces B: Biointerfaces. 2006; 50:1–8.
9. Tokumasu F, Nardone GA, Ostera GR, Fairhurst RM, BEaudry SD, Hayakawa E, Dvorak JA. Altered Membrane Structure and Surface Potential in Homozygous Hemoglobin C Erythrocytes. PLoS ONE. 2009; 4:e5828. [PubMed: 19503809]
10. Wilson W, Wade MM, Holman SC, Champlin FR. Status of methods for assessing bacterial cell surface charge properties based on zeta potential measurements. Journal of Microbiological Methods. 2001; 43:153–164. [PubMed: 11118650]
11. Klodzinska E, Szumski M, Dziuabkiewicz E, Hrynkiewicz K, Skwarek E, Janusz W, Buszewski B. Effect of Zeta Potential Value on Bacterial Behavior during Electrophoretic Separation. Electrophoresis. 2010; 31:1590–1596. [PubMed: 20422634]
12. Rowell RL, Fairhurst D, Key S, Morfesis A, Monahan IM, Mitchnick M, Shattock RA. Microbicides for HIV/AIDS. 1. Electrophoretic Fingerprinting the H9 Cell Model System. Langmuir. 2005; 21:10165–10171. [PubMed: 16229541]
13. Kondo Y, Morita Y, Yamada A, Kimura H. A highly effective method for removing suspended poliovirus from water using a positively charged carbon felt electrode. Microbiology and Immunology. 2004; 488:599–605. [PubMed: 15322340]
14. Riddick, TM. Control of Colloid Stability through Zeta Potential and its Relationship to Cardiovascular Disease. Livingston Publishing; Wynnewood, PA: 1968.
15. Uskoković V, Matijević E. Uniform particles of pure and silica-coated cholesterol. Journal of Colloid and Interface Science. 2007; 315:500–511. [PubMed: 17673225]
16. Uskokovic V. Surface Charge Effects Involved in the Control of Stability of Sols Comprising Uniform Cholesterol Particles. Mat & Manufacturing Processes. 2008; 23:620–623.
17. He X, Li W, Habelitz S. The cooperative self-assembly of 25 and 23kDa amelogenins. Journal of Structural Biology. 2008; 164:314–321. [PubMed: 18845261]

18. Uskokovic V, Castiglione Z, Cubas P, Zhu L, Li W, Habelitz S. Zeta-potential and Particle Size Analysis of Human Amelogenins. Journal of Dental Research. 2009; 89:149–153. [PubMed: 20040742]
19. Wasilewska M, Adamczyk Z, Jachimska B. Structure of Fibrinogen in Electrolyte Solutions Derived from Dynamic Light Scattering (DLS) and Viscosity Measurements. Langmuir. 2009; 25:3698–3704. [PubMed: 19228031]
20. Li W, Gao C, Yan Y, DenBesten PK. X-linked amelogenesis imperfecta may result from decreased formation of tyrosine rich amelogenin peptide (TRAP). Archives of Oral Biology. 2003; 48:177–183. [PubMed: 12648554]
21. Zhu L, Tanimoto K, Robinson S, Chen J, Witkowska E, Hall S, Le T, DenBesten P, Li W. Comparative properties of recombinant human and bovine matrix metalloproteinase-20. Archives of Oral Biology. 2008; 53:785–790. [PubMed: 18336793]
22. Nelson D, Featherstone JD. Preparation, Analysis and Characterization of Carbonated Apatite. Calcified Tissue International. 1982; 34:S69–81. [PubMed: 6293677]
23. Featherstone JDB, Mayer I, Driessens FCM, Verbeeck RMH, Heijligers HJM. Synthetic apatites containing Na, Mg, and CO3 and their comparison with tooth enamel mineral. Calcif Tissue Int. 1983; 35:169–171. [PubMed: 6850399]
24. Shaw WJ, Campbell AA, Paine ML, Snead ML. The COOH Terminus of the Amelogenin, LRAP, Is Oriented Next to the Hydroxyapatite Surface. Journal of Biological Chemistry. 2004; 279:40263–40266. [PubMed: 15299015]
25. Snead ML. Amelogenin Protein Exhibits a Modular Design: Implications for Form and Function. Connect Tissue Res. 2003; 44:47–51. [PubMed: 12952173]
26. Uskoković V, Kim M, Li W, Habelitz S. Enzymatic processing of amelogenin during continuous crystallization of apatite. Journal of Materials Research. 2008; 23:3184–3195. [PubMed: 19177182]
27. Creighton, TE. Proteins: structure and properties. Macmillan Publishers; New York, NY: 2009.
28. Kunz W. The present state of affairs with Hofmeister effects. Current Opinion in Colloid & Interface Science. 2004; 9:1–18.
29. Edwards S. Hofmeister effects in colloid science and biology explained by dispersion forces: analytic results for the double layer interaction. Current Opinion in Colloid & Interface Science. 2004; 9:139–144.
30. Leontidis E. Hofmeister anion effects on surfactant self-assembly and the formation of mesoporous solids. Current Opinion in Colloid & Interface Science. 2002; 7:81–91.
31. Le TQ, Gochin M, Featherstone JDB, Li W, DenBesten PK. Comparative calcium binding of leucine-rich amelogenin peptide and full-length amelogenin. Eur J Oral Sci. 2006; 114:320–326. [PubMed: 16674706]
32. Cazalbou S, Combes C, Eichert D, Rey C. Adaptative physico-chemistry of bio-related calcium phosphates. J Mater Chem. 2004; 14:2148.
33. Bengtsson Å, Shchukarev A, Persson P, Sjo□berg S. Phase Transformations, Ion-Exchange, Adsorption, and Dissolution Processes in Aquatic Fluorapatite Systems. Langmuir. 2009; 25:2355–2362. [PubMed: 19140703]
34. Rosseeva EV, Golovanova OA, Frank-Kamenetskaya OV. The influence of amino acids on the formation of nanocrystalline hydroxyapatite. Glass Phys Chem. 2007; 33:283–286.
35. Barroug A, Lemaitre J, Rouxhet P. Influence of crystallite size on the surface properties of calcium-deficient hydroxyapatites. Journal of Alloys and Compounds. 1992; 188:152–156.
36. Zhang Y, Yokogawa Y. Effect of drying conditions during synthesis on the properties of hydroxyapatite powders. J Mater Sci: Mater Med. 2007; 19:623–628. [PubMed: 17619994]
37. Yao X, Tan S, Jiang D. Fabrication of hydroxyapatite ceramics with controlled pore characteristics by slip casting. J Mater Sci: Mater Med. 2005; 16:161–165. [PubMed: 15744605]
38. Ma J, Liang CH, Kong LB, Wang C. Colloidal Characterization ElectrophoreticDeposition of Hydroxyapatite on Titanium Substrate. Journal of Materials Science: Materials in Medicine. 2003; 14:797–801. [PubMed: 15348400]
39. Sadeghian Z, Heinrich JG, Moztarzadeh F. Preparation of highly concentrated aqueous hydroxyapatite suspensions for slip casting. J Mater Sci. 2005; 40:4619–4623.

40. Tarasevich BJ, Lea S, Bernt W, Engelhard M, Shaw WJ. Adsorption of Amelogenin onto Self-Assembled and Fluoroapatite Surfaces. J Phys Chem B. 2009; 113:1833–1842. [PubMed: 19199690]

41. Aoba T, Fukae M, Tanabe T, Shimizu M, Moreno EC. Selective adsorption of porcine-amelogenins onto hydroxyapatite and their inhibitory activity on hydroxyapatite growth in supersaturated solutions. Calcif Tissue Int. 1987; 41:281–289. [PubMed: 2825935]

42. Tarasevich BJ, Lea S, Bernt W, Engelhard MH, Shaw WJ. Changes in the quaternary structure of amelogenin when adsorbed onto surfaces. Biopolymers. 2009; 91:103–107. [PubMed: 19025992]

43. Zhu L, Tanimoto K, Le T, DenBesten PK, Li W. Functional Roles of Prolines at Amelogenin C Terminal during Tooth Enamel Formation. Cells Tissues Organs. 2009; 189:203–206. [PubMed: 18701806]

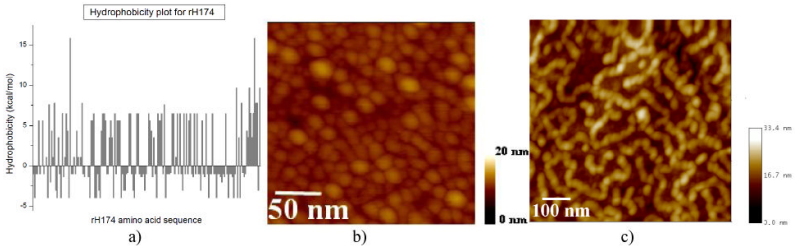

Fig.1.

Hydrophilicity plot for rH174 amino acid sequence calculated using values provided in [Ref. 27] (a), rH174 nanospheres observed in aqueous suspensions (b), and rH174 nanostrings formed by merging of individual nanospheres (c).

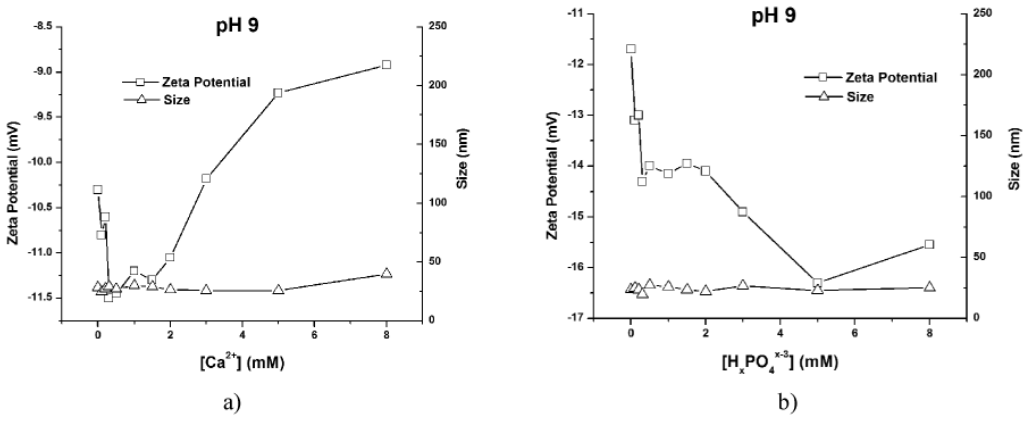

Fig.2.

Hydrodynamic diameters and ζ-potentials of [rH174] = 0.2 mg/ml, 100 mM KCl and 30 mM Tris/Bis-Tris/HCl at pH 9 as functions of $[Ca^{2+}]$ and $[H_xPO_4^{x-3}]$ in the range of 0 - 8 mM.

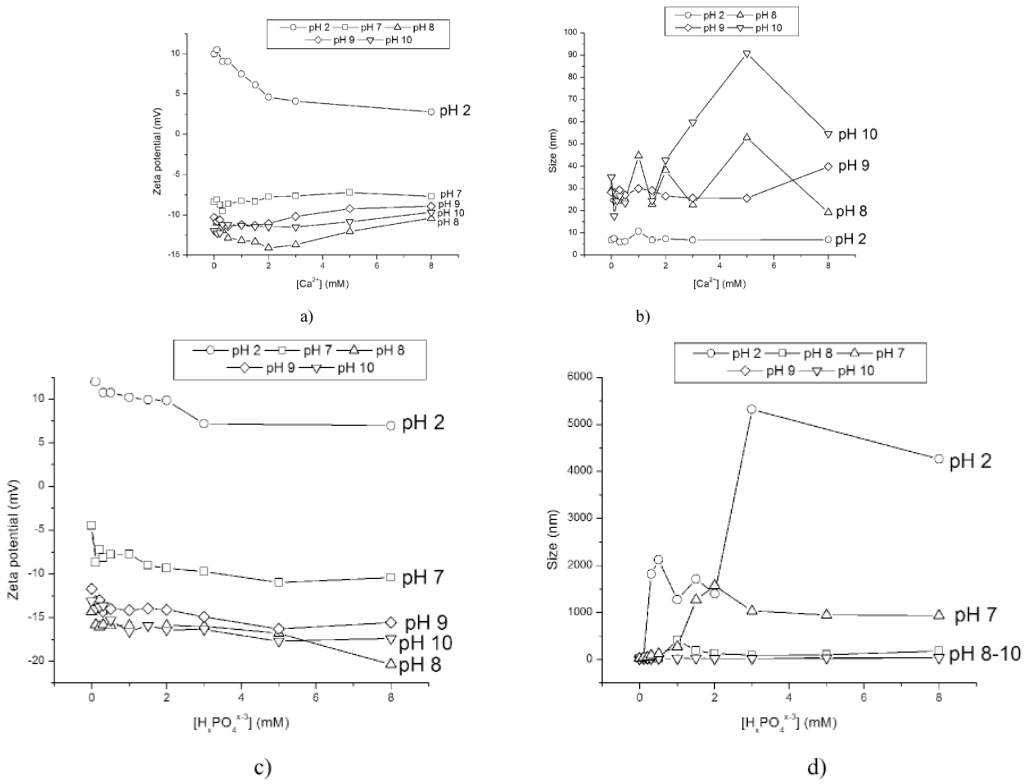

Fig.3.

Hydrodynamic diameters and ζ-potentials of [rH174] = 0.2 mg/ml, 100 mM KCl and 30 mM Tris/Bis-Tris/HCl at different pHs and as functions of $[Ca^{2+}]$ and $[H_xPO_4^{x-3}]$ in the range of 0 - 8 mM.

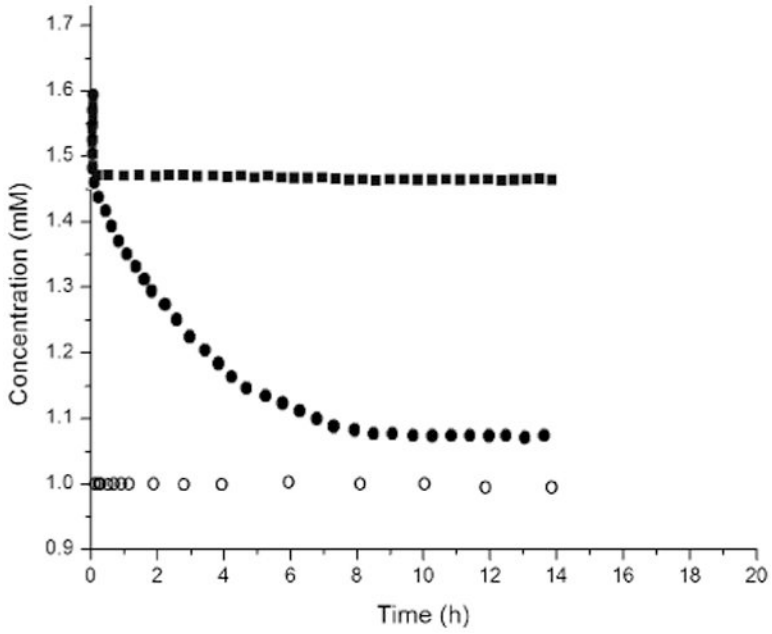

Fig.4.

Concentrations of free Ca^{2+} (●, ■) and $H_xPO_4^{x-3}$ (○) during aging of sols containing: 0.4 mg/ml rH174, 1.6 mM $CaCl_2$, 1.0 mM KH_2PO_4, and 150 mM KCl at 37 °C (●); 0.4 mg/ml rH174, 1.0 mM KH_2PO_4, and 150 mM KCl at 37 °C (○); and 0.4 mg/ml rH174, 1.6 mM $CaCl_2$, and 150 mM KCl, at 37 °C (■).

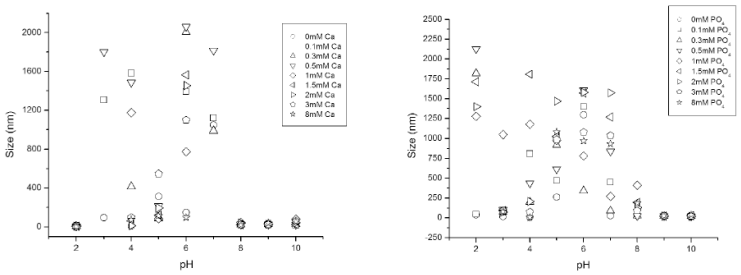

a) b)

Fig.5.

Hydrodynamic diameters of 0.2 mg/ml rH174 in 100 mM KCl and 30 mM Tris/Bis-Tris/HCl at various pHs and concentrations of calcium and phosphate. Ca^{2+} and $H_xPO_4^{x-3}$ concentrations higher than or equal to 1.5 mM are denoted with a star shape.

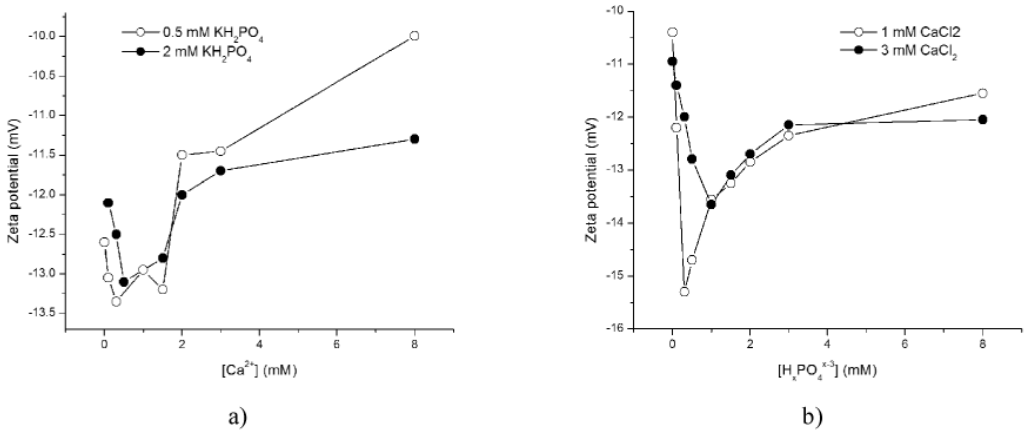

Fig.6.

Effect of adding $CaCl_2$ and KH_2PO_4 to rH174 sols that initially contain different concentrations of KH_2PO_4 and $CaCl_2$, respectively, on ζ-potential of rH174 nanospheres at pH 7.4.

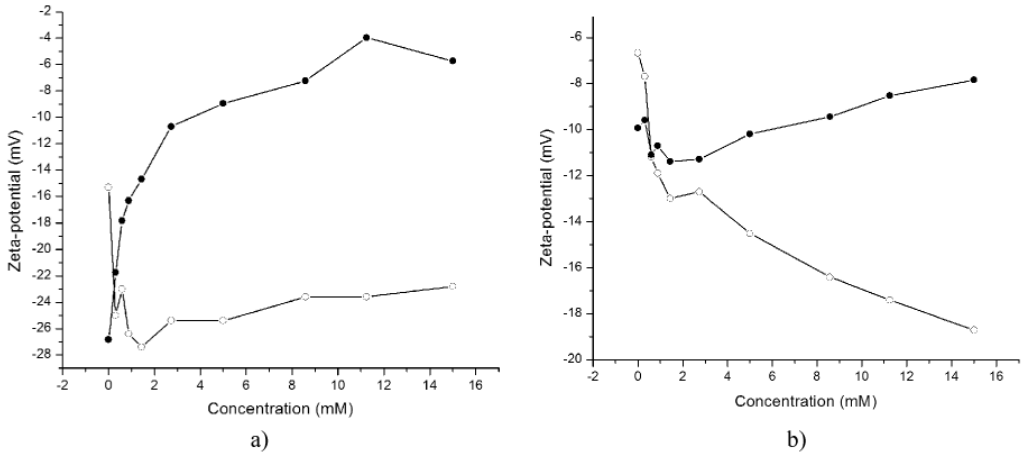

Fig.7.

Change in zeta-potential of HAP (a) and rH174 (b) dispersed in water following the addition of $CaCl_2$ (-●-) and KH_2PO_4 (-○-) up to 15 mM at 25 °C and at pH 7.40 +- 0.02.

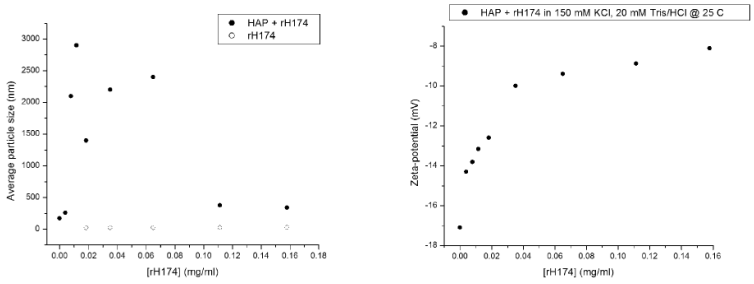

a) b)

Fig.8.

Average hydrodynamic diameter (a) and ζ-potential (b) of pure rH174 and the colloidal mixture of HAP and rH174 at [rH174] = 0 – 0.16 mM when rH174 was added in increments to HAP suspension comprising 150 mM KCl, 20 mM Tris/HCl, at 25 °C and pH 7.4.

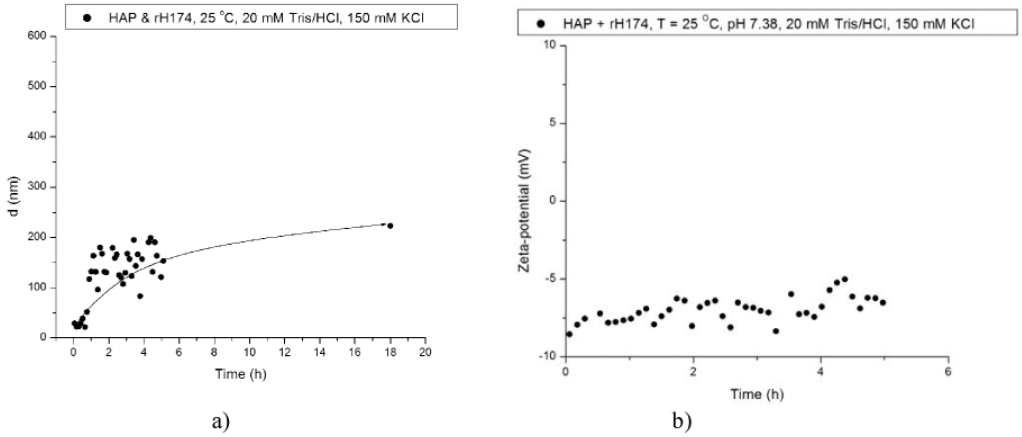

Fig.9.

Average hydrodynamic diameter (a) and ζ-potential (b) of the colloidal mixture of HAP and rH174 at [rH174] = 0.16 mM when rH174 was abruptly added to the HAP sol comprising 150 mM KCl, 20 mM Tris/HCl, at 25 °C and pH 7.40 +- 0.02, and continuously measured over 18 h aging time.

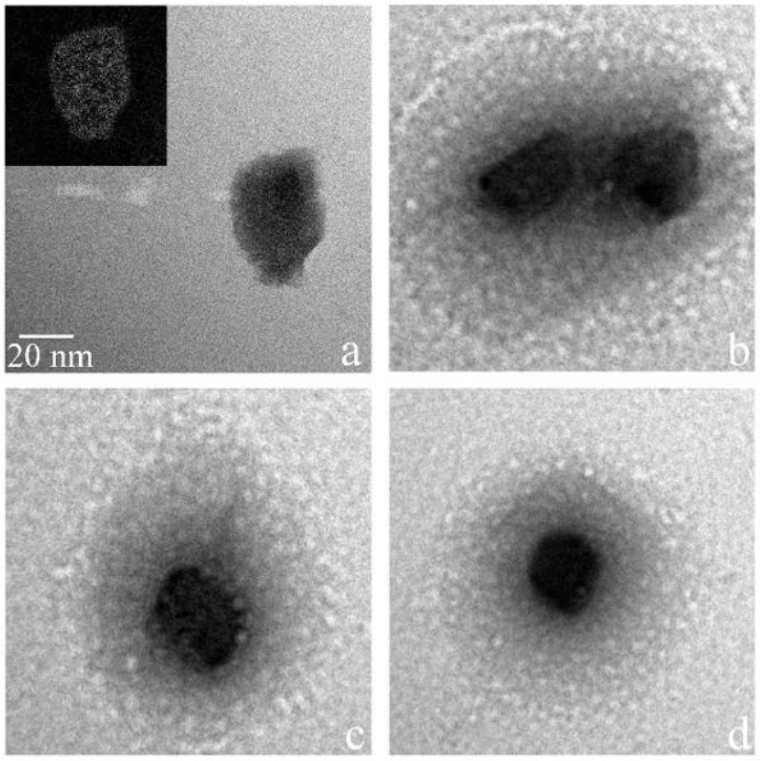

Fig.10.
TEM micrographs of a pure HAP particle suspended in water (a) and HAP particles coated with rH174 upon their mixing and dispersion in aqueous medium (b-d).

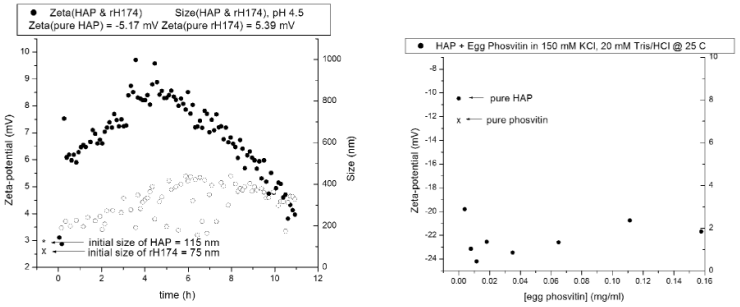

a) b)

Fig.11.

Average hydrodynamic diameter and ζ-potential of the colloidal mixture of HAP and rH174 at [rH174] = 0.16 mM when rH174 was abruptly added to the HAP sol comprising 150 mM KCl, 20 mM Tris/HCl, at 25 °C and pH 4.50 +- 0.02, and continuously measured over 11 h aging time (a), and zeta-potential of HAP/phosvitin mixture at pH 7.40 +- 0.02 (b).